Journal of Materials Chemistry A

ROYAL SOCIETY OF CHEMISTRY

PAPER

View Article Online
View Journal | View Issue

Cite this: J. Mater. Chem. A, 2024, 12, 13852

Effects of partial isovalent substitution of V with (Ti,Fe) on redox reactivity in Li_2VO_2F battery cathodes†

Moritz Hirsbrunner, [a] Ida Källquist, [a] Jolla Kullgren, [b] Håkan Rensmo, [a] Maria Hahlin [ab] and Laurent C. Duda *[a]

We applied photon-only X-ray absorption spectroscopy and resonant inelastic X-ray scattering to study the bulk properties of Li-rich disordered rock salt oxyfluoride cathodes Li_2VO_2F, $Li_2V_{0.5}Ti_{0.5}O_2F$ and $Li_2V_{0.5}Fe_{0.5}O_2F$. We have systematically investigated V 3d- and O 2p-states, both of which are crucial for charge compensation during battery cycling. A combined analysis of both spectroscopies reveals that the vanadium ions deviate from the expected V^{3+}/V^{5+} redox couple for all systems. Moreover, our results suggest that the oxygen ions partake in charge compensation to a considerable degree. Large O 2p-band width changes as a function of doping material are observed. While the diverging trend makes it less plausible that these states have a significant influence on degradation, we find evidence that the presence of O 2p–V 3d hybridized states may constitute a common factor for the previously found improvement in long term cycling of the Ti/Fe-substituted materials. This study demonstrates the power of using a combined spectroscopy approach to understand the tuning properties of Li_2VO_2F to find ways of designing better cathode materials based on this parent compound.

Received 28th September 2023
Accepted 3rd May 2024

DOI: 10.1039/d3ta05916b

rsc.li/materials-a

1 Introduction

In the past decades, the improvement of lithium-ion battery (LIB) technology has revolutionized the energy storage landscape and opened it for widespread application in the electric transportation and portable electronics markets. Still today, cathode capacity is the crucial limiting factor that is sought to be overcome and there is an ongoing quest for novel classes of LIB cathode materials. It has been shown that Li-rich V-oxyfluoride based disordered rock-salts (DRS) are promising materials making use of V^{3+}/V^{5+} redox which lends Li_2VO_2F (LVOF) a high theoretical capacity of 462 mA h g^{-1} (ref. 1 and 2) and experimental first discharge capacity of 330 mA h g^{-1}.[3] However, this material is plagued by fast capacity fading during electrochemical cycling, showing a capacity retention of only 25% to 35% after 50 cycles.[3,4] The structural cycling evolution of this parent material has been thoroughly investigated by X-ray total scattering measurements[5] as well as by X-ray powder diffraction and *operando* total diffraction studies.[6] Thermal stability[7] has been assessed, and the influence of various electrolyte additives on cycling degradation[8] has been evaluated. For oxide materials such as $LiCoO_2$ doping (ion substitution) has been shown to be a powerful strategy to mitigate capacity fading and enhance structural stabilization[9,10] In this context, a recent study has shown that substitution of half of all V in Li_2VO_2F with transition metals (TM) Ti or Fe, *i.e.* $Li_2V_{0.5}Ti_{0.5}O_2F$ (Ti–LVOF), and $Li_2V_{0.5}Fe_{0.5}O_2F$ (Fe–LVOF), significantly increases the capacity retention after 50 cycles to around 70%.[3] The latter study has shown that both Fe- and Ti-substitution in LVOF lead to better long term cycling behaviour, improving coulombic efficiency from 93% (LVOF) to 97% (Ti–/Fe–LVOF) as well as increasing capacity retention after 50 cycles from less than 40% (LVOF) to 66%/73% (Ti–LVOF/Fe–LVOF).[3] The enhanced cycling performance was attributed to a decrease in oxygen activity of the two substituted materials. Additionally, both the Fe and Ti atoms that are substituted into the system can partly participate in the charge compensation process.[3] There are multiple plausible reasons for this observed change in capacity and improved capacity retention. Firstly, the substitution of V with Fe or Ti could suppress the oxygen redox activity that has been observed in these types of materials,[11–13] leading to a more stable structure at the cost of initial capacity. Secondly, the substitution could suppress irreversible side reactions with the electrolyte to form a passivating layer on the cathode.[14–16]

It is intriguing that substitution of V in LVOF with 3d transition metals from opposite directions in the 3d-row of the periodic table effectively leads to similar electrochemical

[a]Department of Physics and Astronomy, Division of Molecular and Condensed Matter Physics, Uppsala University, Box 516, 751 20 Uppsala, Sweden. E-mail: laurent.duda@physics.uu.se

[b]Department of Chemistry – Ångström Laboratory, Uppsala University, Box 523, 751 20 Uppsala, Sweden

† Electronic supplementary information (ESI) available. See DOI: https://doi.org/10.1039/d3ta05916b

cycling improvements. This is puzzling, for instance when considering the opposing effects on the ionic radius of the substitutional ions. This prompts the question whether a single common cause can be found to explain the observed improvements by substitution. It is timely and valuable to scrutinize the effect of such substitution of the electronic structure of the primary and common active constituents in all of the systems, namely oxygen and vanadium. Our study therefore aims at carefully studying and locating the salient effects that transition metal substitution has on important properties of the electronic structure of the LVOF system.

It has been shown that considerable differences exist between near-surface and bulk reactions in the active material.[4] The roughly spherical active-material particles have a core–shell structure with respect to their electronic structure. There is evidence for degradation that propagates from the surface layers into the bulk, whereby oxygen redox reactions were identified as an important initiating culprit. Mapping and distinguishing the surface *versus* bulk contributions is important for the understanding of degradation of the material. This has been partially addressed in previous electronic structure analysis that applied HAXPES,[3] a technique with a probing depth of up to about 10 nm, however it essentially monitors layers that still are affected by the surface vicinity. In this work, we employ purely photon-based V $L_{2,3}$- and O K-edge XAS and RIXS with a typical probing depth of 100 nm, rendering the spectra virtually free from surface effects.[17,18]

Here, we present V $L_{2,3}$- and O K-edge XAS and RIXS of the cathodes Li_2VO_2F, $Li_2V_{0.5}Ti_{0.5}O_2F$ and $Li_2V_{0.5}Fe_{0.5}O_2F$ during the initial cycle. We analyze the electronic structure of these two constituents that are responsible for the main part of the charge compensation. We observe that substitution affects both V- and O-states at binding energies over several electron volts. Intriguingly, we observe strong trends regarding the width as well as the energy positions of O 2p-derived bands. While the diverging trend appears to exclude the oxygen bandwidth as a common factor to the observed improvements in capacity retention by substitution of Fe or Ti, we argue that the behaviour of states closer to the Fermi level may have a greater significance. We observe that substitution of V in Li_2VO_2F both for $Li_2V_{0.5}Ti_{0.5}O_2F$ and $Li_2V_{0.5}Fe_{0.5}O_2F$ show lower levels of these states compared to the parent compound. Thus we conclude that maintaining a reduced level of such states may have significance for improving capacity retention in Li-rich V-oxyfluoride cathodes.

We also refine the range of vanadium redox in the bulk, finding that it does not account for the entire charge compensation in the materials as previously attributed to a perfect V^{3+}/V^{5+} redox couple. Rather, we find that oxygen states play a significant role in charge compensation.

2 Methods

2.1 Synthesis and electrochemistry

The battery cathode active materials were made using a planetary ball mill (Fritsch Pulverisette 6 classic line) and metal oxide precursors (Alfa Aesar) in a two step process. First, Li_2O was combined with V_2O_3 and either Ti_2O_3 or Fe_2O_3 and milled to form the intermediate compounds $LiVO_2$, $LiV_{0.5}Ti_{0.5}O_2$ and $LiV_{0.5}Fe_{0.5}O_2$ respectively. Secondly, by adding LiF to the milling process, the final cathode materials Li_2VO_2F, $Li_2V_{0.5}Ti_{0.5}O_2F$ and $Li_2V_{0.5}Fe_{0.5}O_2F$ were formed. Each ball milling step was run for 20 h at 600 rpm using a 10 : 1 ball to powder ratio. All materials were handled in a argon-filled glovebox and transferred to an air-tight jar for the milling process. The electrodes were made by combining the active material with carbon black and the binder polyvinylidene difluoride (PVdF) in a 70/20/10 weight%-ratio. The resulting slurry was coated onto an aluminum foil and dried in vacuum for 12 hours under increasing temperature, rising up to 120 °C. The final active material mass loading on the cathode was approx. 1.5 mg cm^{-2}. This sample synthesis process follows the same procedure as was used by Baur *et al.*[3]

Electrochemical measurements were carried out in a half cell configuration using the sample electrode material as working electrode, lithium metal as counter electrode, glass fiber separators (Whatman) and 200 μl LP30-electrolyte (1 M $LiPF_6$ in a 1 : 1 volume ethylene carbonate/dimethyl carbonate (EC/DMC) mixture). Assembly and vacuum sealing of the pouch-type cells was done in an argon-filled glovebox. Battery cycling was conducted using an ARBIN BT2000 battery testing system, applying a C/5 rate in a voltage range of 1.3 V to 4.1 V at room temperature.[3,4] Three samples of each of the three material systems Li_2VO_2F (LVOF), $Li_2V_{0.5}Fe_{0.5}O_2F$ (Fe–LVOF), and $Li_2V_{0.5}Ti_{0.5}O_2F$ (Ti–LVOF), were produced to investigate the materials at varying states of charge (SoC). They are: pristine, 'end of charge' (EoC) which were charged to 4.1 V, also referred to as 'delithiated', and 'end of discharge' (EoD) which were discharged to 1.3 V after being charged to 4.1 V, also referred to as 're-lithiated'.

2.2 X-ray spectroscopy

V $L_{2,3}$-edge and O K-edge X-ray absorption spectroscopy (XAS) and resonant inelastic X-ray scattering (RIXS) spectra from *ex situ* cathodes were obtained at the beamline BL27SU at Spring 8, Japan.[19,20] The cathodes were obtained by disassembling battery cells cycled at our home lab. Pieces of cathodes were extracted in Ar glove boxes, sealed and shipped air-tight. At the beamline, the samples were opened in an Ar glove box, transferred to a vacuum suitcase and inserted to the X-ray spectroscopy measurement chamber without contact to ambient atmosphere at any instance. Partial fluorescence yield (PFY) spectra were measured at a resolution of about 0.1 eV. PFY was detected using an energy dispersive silicon drift detector (SDD). Oxygen K-edge RIXS spectra were recorded with a spectrometer of a varied-line-spacing plane cylindrical grating design in first order of diffraction at a combined resolution of about 0.4 eV. The vertical (horizontal) beam size at sample point was about 10 μm (200 μm).

Additional high-resolution V $L_{2,3}$-edge and O K-edge RIXS spectra of Li_2VO_2F and $Li_2V_{0.5}Fe_{0.5}O_2F$ were collected at the ADRESS – X03MA beamline at the SLS, Villigen-PSI, Switzerland utilizing the Super Advanced X-ray Emission Spectrometer

(SAXES).[21,22] SAXES consists of a VLS spherical grating and a CCD detector with an adjustable detection range of 0.4–1.6 keV with a resolution of 10 000, *i.e.* 50 meV at 500 eV and 100 meV at 1 keV.

2.3 Theory

Atomic-multiplet calculations of vanadium $L_{2,3}$-edge RIXS were carried out using Quanty[23] run on the graphical user interface Crispy.[24] The parameters for the calculations were chosen from de Groot *et al.*[25] for V^{3+} and V^{4+} in O_h symmetry. The crystal field parameter ($10Dq$) was iterated to find a good agreement with the experimental results.

3 Results

3.1 X-ray absorption

In Fig. 1, we show V $L_{2,3}$- and O K-edge XAS spectra in partial fluorescence yield mode (PFY) for the three different cathode systems LVOF, Fe–LVOF and Ti–LVOF. Spectra of different states of charge (SoC) of the first cycle are overlayed: pristine, delithiated/EoC, and re-lithiated/EoD and vertically offset between samples for clarity. V $L_{2,3}$-edge and O K-edge spectra are split up into different subplots (a) and (b), in which the V $L_{2,3}$- and O K-edges are normalized to their respective atomic steps, thereby eliminating the intensity differences between samples due to different V/O ratios. Vertical dotted lines show the incident energies chosen for the RIXS measurements presented further below. Note that the pristine V $L_{2,3}$-edge Fe–LVOF spectrum showed an intensity irregularity from the measurement (light grey region in Fig. 1a) which was normalized by comparing the data with the PFY made from the RIXS spectra, the process of which is described in detail in the ESI with Fig. ESI 1.† The salient features from the V $L_{2,3}$-edge in Fig. 1a can be summarized by the following: (i) a small peak between the L_3 and L_2 regions at roughly 521 eV which has been connected to the V^{3+} oxidation state,[25–27] (ii) a spectral weight shift within the L_3 peak from the lower energy peak (roughly 517 eV) to the higher energy peak (roughly 518 eV), indicating a higher oxidation state of V,[25,28] (iii) an overall shift of the $L_{2,3}$ region towards higher energies which has been found to be a sign of oxidation of the V atoms.[25,27–29]

Fig. 1b shows the O K-edge XAS of all cathode systems and reflects the anionic activity at the oxygen ions during cycling. For LVOF (top traces), delithiation leads to a narrowing of the prepeak region (529–535 eV), *i.e.* the oxygen contribution to the conduction band, and an increase in hole states in the band closest to the Fermi level. For Ti–LVOF (middle traces) the trend is similar, whereas in the pristine cathode this band is completely filled (nearly zero XAS intensity). The spectrum of delithiated Ti–LVOF (yellow trace) appears shifted to lower energy (arrow) or, in other words, we observe an intensity increase from zero at energies close to the bottom of the conduction band. For Fe–LVOF (bottom traces) we observe very little overall spectral shape variation upon delithiation (similar as for V $L_{2,3}$-edge XAS). Regarding relithiation in the cathode materials, we find that there is a high level of recovery in

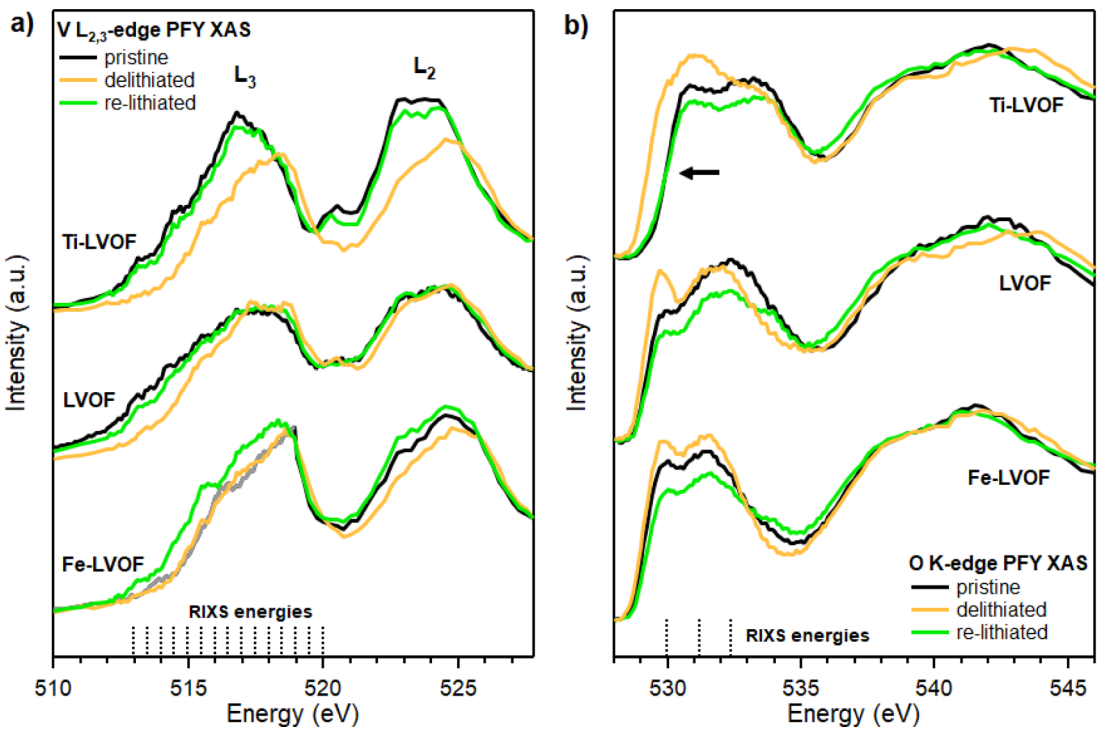

Fig. 1 State of charge comparison (lithiated/delithiated) of XAS spectra during the first cycle. PFY mode XAS of V $L_{2,3}$-edge (a) and O K-edge (b) of Ti–LVOF (top), LVOF (middle) and Fe–LVOF (bottom), respectively. Spectra are shown for different states of charge (SoC) within the first cycle: pristine in black, end of charge (EoC/delithiated) in yellow, and end of discharge (EoD/re-lithiated) in green. The spectra of the different sample systems are offset along the intensity axis for clarity.

spectral shape toward the pristine state while the intensity of the pre-peak decreases for all three materials.

We have not found any evidence for oxygen redox in any of the LVOF systems of the kind that has been recently observed in other Li-rich materials.[30–33] Previous reports of reversible evolution of molecular oxygen (O_2) during the redox reaction have found vibrational signatures close to the elastic peak as well as an energy loss peak at around −7.5 eV in the O K-edge RIXS spectrum of such molecular oxygen. Neither of these features were observed in the RIXS spectra (see Fig. ESI 3†). On the other hand, the present O K-edge XAS and RIXS spectra reveal other types of anionic activity with a magnitude that is highly dependent on the dopant material and where anionic activity is smallest for Fe–LVOF and largest for Ti–LVOF, yet most reversible for the latter.

3.2 O K- and V $L_{2,3}$-edge RIXS

In Fig. 2, the V $L_{2,3}$-edge RIXS spectra of the different material systems at varying states of charge are overlayed. The upper panel shows the spectra taken at SPring-8, Japan, while the lower panel shows high resolution V $L_{2,3}$-edge as well as O K-edge RIXS spectra of Fe–LVOF samples that were obtained at the SLS, Switzerland. The spectra can be grouped into two regions in addition to the elastic peak at 0 eV energy loss. Firstly, the area between −1 eV and −4 eV (shaded turquoise) corresponds to dd-excitations in the vanadium, and secondly the area beginning at −5 eV (shaded pink) corresponds to charge transfer (CT) excitations.[34] The CT excitations belong to energy loss states that are more delocalized owing to the hybridization of the vanadium 3d-orbitals and the oxygen 2p-orbitals. By contrast, the dd-excitations involve the localized d-orbitals of the vanadium ions. Calculated RIXS spectra resulting from dd-excitations in V^{3+} and V^{4+} are also displayed in the figure. They were calculated based on parameters used by de Groot *et al.*[25] The crystal field parameter ($10Dq$) was set to 1.9 eV and 1.5 eV for V^{3+} and V^{4+} respectively.

We find that the Fe–LVOF samples show a higher intensity of the CT-peak region, *i.e.* delocalized states, compared to the other materials. The position of the center of gravity of the CT-peak in the pristine samples is pointed out by the respective dotted lines and correspond to −8.64 eV for Ti–LVOF, −8.22 eV for LVOF, and −7.6 eV for Fe–LVOF. Upon delithiation the centers of gravity of the CT-peaks shift towards lower energy loss in all materials and align at −6.18 eV (marked by the long dotted line in Fig. 2). The Ti–LVOF material shows the lowest CT excitation intensity located at the highest energy losses. This correlates with the already higher oxidation state of vanadium in Fe–LVOF material in its pristine condition. Thus the other materials move closer to this state upon delithiation. This corroborates the observation made in the O K-edge XAS, where Ti–LVOF shows a large energy shift when comparing the pristine/re-lithiated samples to the delithiated sample where the latter shifts towards the same energy as observed for the LVOF and Fe–LVOF. Importantly, this process is observed to be reversible during the first cycle.

The bottom panel of Fig. 2 shows that our high resolution RIXS data of Fe–LVOF fully support the more complete set of

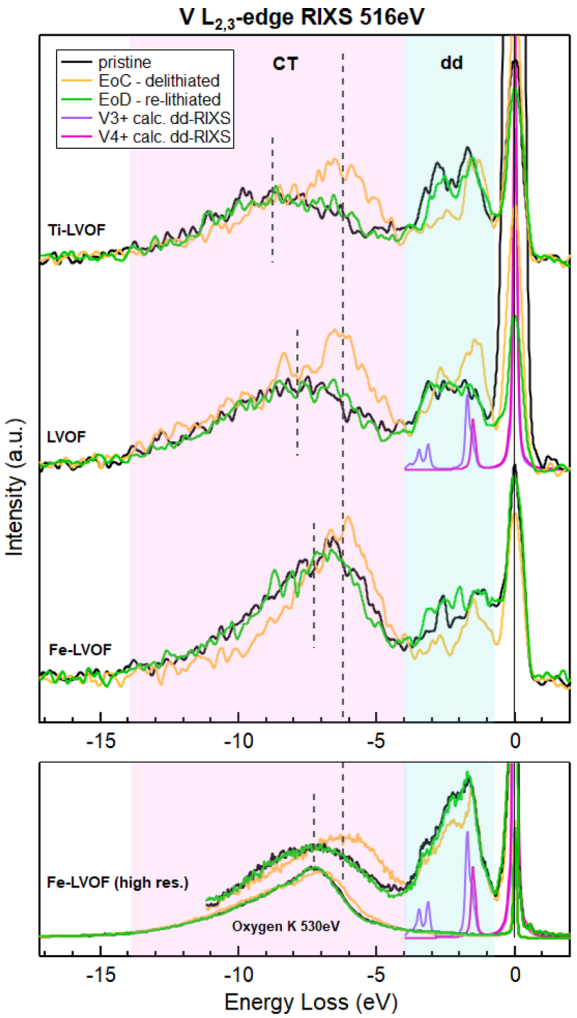

Fig. 2 State of charge (lithiated/delithiated) comparison of the V $L_{2,3}$-edge RIXS spectra taken at 516 eV of Ti–LVOF, LVOF, Fe–LVOF (top box) and high resolution V $L_{2,3}$-edge and O K-edge spectra of Fe–LVOF taken at 516.4 eV (bottom box). Spectra are offset on the intensity axis for clarity. For each material the different states of charge are displayed. Additionally, calculated dd-RIXS spectra are shown for V^{3+} and V^{4+}. Color-shading indicates dd- and CT-peaks, respectively. Vertical dashed lines indicate approximate CT-peak positions for convenience.

lower resolution data. The high resolution V $L_{2,3}$-edge RIXS spectrum aligns well with its lower resolution counterpart and reflects the same trends. Additionally, this figure illustrates how CT excitations at the vanadium $L_{2,3}$-edge overlap with the oxygen K-RIXS main band. The two excitations are connected as the CT excitations are a result of hybridization with its oxygen ligand. We point out that both peaks reveal the same behaviour in shifting towards lower energy loss upon delithiation. Finally, this figure shows where V 3d-hybridized states may be expected in the low-intensity O 2p-band in the energy loss region 0–5 eV. We will discuss these in more detail below.

Turning to Fig. 3, the O K-edge RIXS spectra for an incidence photon energy 530 eV are shown comparing the sample materials in dependence of state of charge (pristine, delithiated, re-lithiated). Spectra are offset on the intensity scale for clarity.

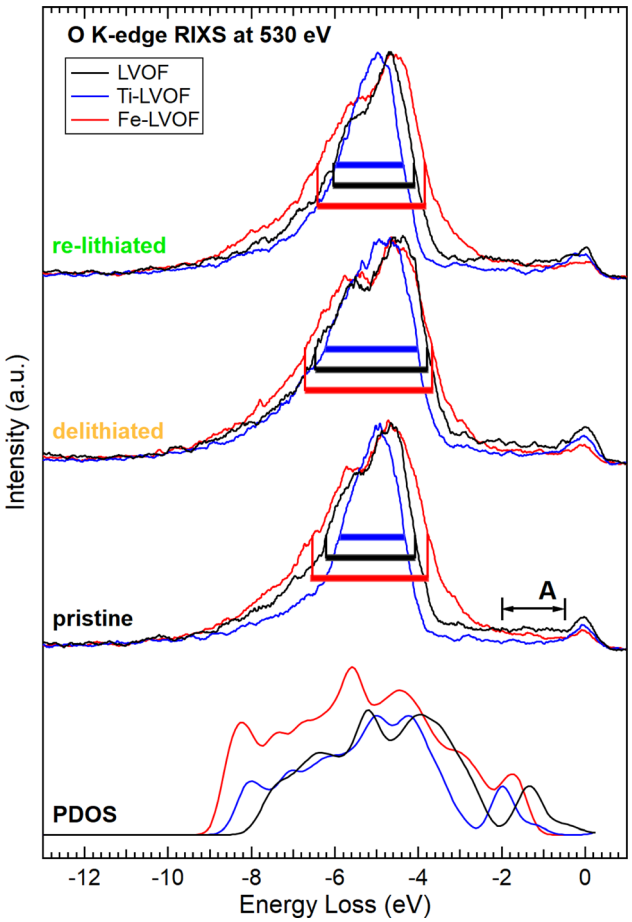

Fig. 3 Dopant dependence of O K-edge RIXS spectra of samples at different states of charge (vertically offset): pristine, delithiated (EoC), and relithiated (EoD), calculated partial density of states (PDOS) of oxygen for pristine materials. A RIXS excitation energy of 530 eV was chosen. Colored boxes indicate the FWHM of the corresponding peak.

Our DFT calculations of the occupied oxygen PDOS for the pristine LVOF, Fe–LVOF and Ti–LVOF are also shown for comparison on the bottom of the graph. The O K-edge RIXS can serve as an approximate representation of the density of states of the occupied states below the Fermi level.[35] The width of the RIXS peak can therefore be understood as indicating an overall width of the oxygen band below the Fermi level. From the O K-edge RIXS, we determined values for the full width at half maximum (FWHM) of the low energy peak for the spectra taken at 530 eV. They are shown in Table 1. The O K-RIXS main band shows dramatic variations in width for the three different sample systems. For all stages of cycling, Ti–LVOF displays the narrowest peak, the LVOF peak being slightly wider, and Fe–LVOF showing the broadest peak overall. The calculated oxygen PDOS reflects this tendency in the changing peak width very clearly. We can therefore see the correspondence of the width of the RIXS peak to the width of the 2p band. Additionally to the doping dependent variation of the pristine materials, we observe that cycling of the electrodes leads to a change in the FWHM of the oxygen RIXS peak. The peaks FWHM grows upon delithiation by 0.6 eV in Ti–LVOF and LVOF and by 0.3 eV in Fe–LVOF, and subsequently becomes smaller again during re-lithiation (−0.6 eV for Ti–LVOF, −0.7 eV for LVOF, and −0.5 eV for Fe–LVOF).

Table 1 FWHM of the main energy loss peak in the O K-edge RIXS spectra shown in Fig. 3. The uncertainty was estimated to be ±0.1 eV

	Sample		
SoC	Ti–LVOF	LVOF	Fe–LVOF
Pristine	1.6 eV	2.1 eV	2.8 eV
Delithiated	2.2 eV	2.7 eV	3.1 eV
Re-lithiated	1.6 eV	2.0 eV	2.6 eV

We now turn to the low-intensity region within a few eV of the elastic peak, denoted as region A in Fig. 3. These low-energy states can be observed for all samples with varying intensity. We attribute these excitations to states related to O 2p- TM 3d hybridization, mainly V 3d-states. To compare these states between materials, we formed and compared averaged intensity values in the energy range between 0.5 eV and 2 eV energy loss relative to the intensity of the main peak at 5 eV energy loss revealing increasing intensity in the following order: Ti–LVOF, Fe–LVOF, LVOF. This can be compared to the oxygen PDOS in the same energy region shown on the bottom of Fig. 3. Here we rather see a difference in energy position of the low-lying peak where LVOF shows the highest energy position, followed by Fe–LVOF and then Ti–LVOF.

4 Discussion

The substitution of V with Fe/Ti has been found to improve the structural stability of the material.[3] On the other hand, our XAS and RIXS results show that partial replacement of V by Fe and Ti in LVOF strongly influence both V 3d-as well as O 2p-states, both of which are crucial for charge compensation during battery cycling. This underlines the powerful potential of substituting V for tuning the properties of LVOF in the desired direction to obtain better cathode materials based on the parent compound.

4.1 Oxygen bandwidth and low-energy states

Regarding the question whether there may exist commonalities in the improved properties and changes in the electronic structure, the most striking observation in this respect might be considered to be the variation of the width of the O K-RIXS main peak. This implies a strong sensitivity of the oxygen valence band (Fig. 3) to the substitution of V by Fe and Ti in LVOF. The observed FWHM of the oxygen peak is summarized for all samples in Table 1. We find that the parent compound LVOF exhibits an O 2p-band width that lies between Ti–LVOF and Fe–LVOF, following the expected 3d TM trend. Thus the width of the O 2p-band does not appear to correlate simply with the performance or degradation behaviour of the different materials. We recall that the cycling performance as well as capacity retention was found to be enhanced for both Fe–LVOF and Ti–LVOF while the bandwidth is found to change in opposite directions. Instead, the observed width change can be explained by the increase of d-band electrons when moving from Ti to V and then to Fe.

While O 2p bandwidth changes of the pristine materials are dopant-dependent, there are also large width changes that depend on SoC, *i.e.* lithiation degree, within each sample system. Intriguingly, the bandwidth changes opposite to the expected tendency when electrons are removed during charging. A simple picture in which electrons are removed from the O 2p band, and therefore involves fewer occupied valence states, would suggest that the O 2p-band would become more narrow, instead the opposite occurs.

Despite the strong variation of the width of the main oxygen band, it is probably not the common factor that determines the cycling improvement due to substitution. Notably, the O 2p states discussed above are several electron volts below the Fermi level, and therefore may be chemically less relevant. Instead, other states and their initial presence in the pristine materials may be more relevant and help predict long term performance. These are states closer to the Fermi level, namely the region close to the elastic peak of the O K-RIXS (Fig. 3 region A). They are a result of hybridization between the oxygen 2p-states with transition metal 3d-states. It is important to note that, this study focuses on the vanadium states, but the d-states from substituted metals (Fe,Ti) could play a role as well. Our study might then suggest that materials, such as Fe–LVOF and Ti–LVOF with fewer such states close to the Fermi level are generally also the ones with better long term cycling stability. Thus, a way of improving the understanding of substituted LVOF-based materials in general appears to lie in the identification and study of such states in since they could be crucial to degradation processes and long-term cycling stability.

4.2 Band movement of V 3d–O 2p hybridized states

The O K-edge XAS (see Fig. 1) reveals additional differences in electronic structure behaviour between the Ti–LVOF and Fe–LVOF cathode systems during cycling. Consider the pre-peak of the pristine and delithiated samples of the three sample systems (see the arrow in Fig. 1). Interestingly, there is an apparent shift to higher excitation energy for the Ti–LVOF system upon delithiation. Upon closer inspection, all cathode systems appear to possess a narrow region/peak at the leading edge whose intensity varies with degree of lithiation, being strongest for Ti-doped LVOF. We attribute this region to V 3d/O 2p-hybridized states. This behaviour is paralleled by the V $L_{2,3}$-edge RIXS spectra (Fig. 2), namely the shift of the center of gravity of the CT excitations. This harmonized similarity of this trend to the O K-edge XAS state with the CT excitations of vanadium are a result of the hybridization of the V atom with the oxygen ligands. All three cathode systems have a common trend that delithiation causes the CT-peak to shift towards lower energy loss (indicated by the dotted lines) when they align in energy. We find the largest such shift for Ti–LVOF, matching the strongest apparent shift of the O K-edge spectra, and the smallest shift for Fe–LVOF.

4.3 Oxidation states of V ions

The V $L_{2,3}$-edge XAS data (Fig. 1a) provides us with a means to evaluate the oxidation state of the vanadium atoms in the bulk of the different materials depending on the state of charge by investigating salient features and comparing with the literature. This is summarized in Fig. 4. Although the present results are in broad agreement with a previous report on these materials using complementary X-ray spectroscopies[3] we find noteworthy deviations from the proposed V^{3+}/V^{5+} redox couple for all systems.

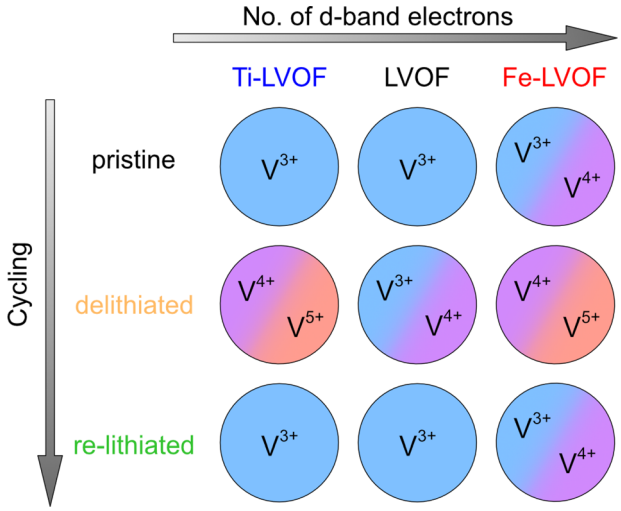

Fig. 4 Proposed oxidation state of the vanadium inside the samples in different states of charge derived from the XAS spectra in Fig. 1.

The V $L_{2,3}$-edge spectra reveal that all systems experience a shift of the V $L_{2,3}$ peaks to higher energies upon delithiation, which is a typical behaviour for V oxidation. However, this shift is significantly larger for Ti–LVOF compared to LVOF and Fe–LVOF. There is a significant variation, where both pristine LVOF and Ti–LVOF show a small peak at 521 eV, revealing the presence of V^{3+}, while the peak is absent in the Fe–LVOF spectra. Therefore, already the pristine Fe–LVOF can be assumed to contain V in an oxidation state between V^{3+} and V^{4+}.

For delithiated Ti–LVOF the peak related to V^{3+} at 521 eV disappears, shifting its oxidation state to at least V^{4+}, whereas the peak is still visible for LVOF, meaning that oxidation in Ti–LVOF is stronger than for LVOF which retains some V^{3+} during delithiation. Furthermore, there is a clear shift in spectral weight in the $L_{2,3}$ peak to the higher energy side visible in Ti–LVOF that is much less noticeable in Fe–LVOF and even smaller still for LVOF. From this we infer that vanadium in Ti–LVOF undergoes the strongest oxidation of the three materials.

Regarding Fe–LVOF, we observe a small total energy shift as well as a small shift in spectral weight. Additionally, the decrease in $L_{2,3}$-peak intensity can also be interpreted as a sign for substantial oxidation suggesting that the delithiated ions are in a state between V^{4+} and V^{5+}. Turning to the relithiated cathodes, we find diverse behaviours. Ti–LVOF shows the best reversibility, returning nearly completely to the pristine state while LVOF and Fe–LVOF behave comparably more irreversible but still mostly recover their pristine shape. Based on these features, we propose oxidation states of the sample systems at different SoC as depicted in Fig. 4. Notably, the vanadium in

LVOF does not follow the expected V^{3+}/V^{5+} redox couple, instead showing lower amounts of oxidation.

The observations made in the XAS are complemented by the V $L_{2,3}$-edge RIXS shown in Fig. 2 together with results of atomic multiplet calculations of dd-RIXS spectra for V^{3+} and V^{4+}. The dd-excitations, highlighted with a light-blue background, give insight about the intra-band behaviour of the valence d-band electrons. In case of V^{5+} we reach the $3d^0$ configuration, *i.e.* there are no electrons left over in the d-band. Consequently, there would be no signal in the RIXS in the dd-region. From this we can confidently assert that none of the samples reach a pure V^{5+} state, as all of them still show some intensity in the region of dd-excitations. The calculations for V^{4+}, with a single electron in the d-band ($3d^1$), render only one excitation peak in the RIXS spectra. Delithiation leads to the enhancement of the lower-lying V dd-excitation in all three materials, most evident for Ti–LVOF, suggesting a higher admixture of V^{4+} states for this SoC. The calculations for V^{3+} leads to a more richly structured spectrum due to the presence of two electrons in the d-band which can clearly be observed in the experimental spectra for lithiated cathodes.

Additionally, a shift between the dd-features of the V^{3+} and V^{4+} can be observed in the experimental spectra, that can be accounted for by a change in the crystal field of the two vanadium ions from 1.9 eV in V^{3+} to 1.5 eV in V^{4+} in the calculations. However, there is unaccounted for intensity visible in the experimental spectra between the two proposed regions from the calculated V^{3+} dd-RIXS. This could be a result of the O_h-symmetry being broken to some degree in the material, *e.g.* in case of structural deformation that occurs during cycling.

While the absolute intensity observed in a RIXS spectrum depends on may factors, the observed ratio between CT-peak and dd-peak can inform about the oxidation state trends,[36] where a higher CT-to dd-intensity ratio indicates a higher oxidation state. This is particularly useful for discussing the delithiated cathodes. Thus based upon the observation that the ratio between CT-peak and dd-peak is significantly larger for Fe–LVOF than the other systems, we conclude that delithiated Fe–LVOF contains a higher ratio of V^{5+} to V^{4+}. For delithiated LVOF, we come to the conclusion that it is in a mixed state of V^{3+}/V^{4+}. This is derived from the fact that there are clearly two peaks in the dd-excitation region, where the lower energy loss peak has a significantly increased intensity, a sign for V^{4+}. The resulting change in oxidation state is surprisingly low considering its measured discharge capacity of 330 mA h g^{-1} (discussed more below).

The degree of cycling reversibility can be assessed by how well the spectra of the re-lithiated cathodes match with the ones of the corresponding pristine material. Here, Ti–LVOF reveals to be the most reversible, reverting back to its initial state almost completely during the first cycle while LVOF and Fe–LVOF show comparatively more irreversibility. For the calculation of the theoretical capacity of 462 mA h g^{-1}, the full oxidation/reduction of the V^{3+}/V^{5+} redox couple was assumed.[1,2] In the case of the previously experimentally observed discharge capacity of 330 mA h g^{-1} this necessitates the transfer of 1.4 Li^+ per V atom leading to an average oxidation state of $V^{4.4+}$ after delithiation.[3] However, the clear observation of V^{3+} in the delithiated sample as well as a lower energy shift and spectral weight shift compared to the substituted materials suggests an active participation of oxygen in the charge compensation and perhaps a partly heterogeneous redox process leading to coexistence of V^{3+} and V^{5+}. For Ti- and Fe–LVOF, while the initial discharge capacity is significantly lower (285 mA h g^{-1} and 218 mA h g^{-1} respectively), substitution of half of the V means that even more than 1.4 Li^+-ions are transported per available V atom when considering no/low participation of the Fe/Ti ions as was previously proposed.[3] While a stronger redox behaviour can be observed in these materials, it is not strong enough to account for the full V^{3+}/V^{5+} redox. In this case, apart from the participation of oxygen this could mean that the substituted Ti,Fe-ions participate more in the charge compensation process than previously assumed.[3]

5 Conclusion

Using the bulk sensitive techniques RIXS and XAS, we investigated the promising battery cathode material Li_2VO_2F, as well as materials partly substituted with Fe ($Li_2V_{0.5}Fe_{0.5}O_2F$) and Ti ($Li_2V_{0.5}Ti_{0.5}O_2F$).

We find that vanadium redox activity in the materials depend strongly upon the substitutional element (Ti or Fe). The V $L_{2,3}$-edge XAS reveals that Ti–LVOF exhibits both the best reversibility as well as the largest V-redox activity out of the three sample systems, while we note that pristine Fe–LVOF starts already at a higher initial V oxidation state (V^{3+}/V^{4+}) than the other systems. Additionally, the contained vanadium does not follow the proposed V^{3+}/V^{5+} redox couple,[3,4] instead showing lower amounts of oxidation/reduction. This suggests significant participation of the oxygen in Li_2VO_2F as well as stronger participation of the Ti and Fe than previously expected in the substituted materials.

While a previous study has shown that partial substitution of V by Fe or Ti both leads to an improved cycling stability of the material,[3] a possible explanation for an underlying common factor has been elusive. The present O K-edge RIXS results reveals a significant diverging behaviour of the O 2p-band width in Fe–LVOF (broadening) and Ti–LVOF (narrowing) compared to LVOF, which suggests that O valence bandwidth is not necessarily connected to better long term cycling performance. Instead, states close to the Fermi level coming from the hybridization of O 2p-with TM 3d-states could be a pointer for cycling degradation. We observe in the O K-RIXS that the substituted materials Fe–LVOF and Ti–LVOF have fewer such states than the parent compound LVOF. Therefore we conclude that these states could be of importance to the structural stability during cycling of the cathode material.

Conflicts of interest

There are no conflicts to declare.

Acknowledgements

The authors acknowledge the financial support from the Swedish Energy Agency to the projects "X-ray based

methodology for next generation Na-ion battery cathodes" (project number: 50745-1) and "Ageing of Lithium-ion Batteries with Nickel-Rich Cathodes for Electromobility" (project number: 45538-1), the Swedish Research Council (project number: 2018-06465 and 2022-06076), as well as StandUP for Energy consortium, Sweden. We thank K. Tsuruta for excellent technical support at BL27SU of SPring 8 (proposal no. 2018B1474) and the group of Th. Schmitt for assistance at the ADRESS beamline of the Swiss Light Source at the Paul Scherrer Institute (PSI), as well as F. Massel for his contribution in the sample handling and data acquisition during the beamtime.

Notes and references

1 R. Chen, S. Ren, M. Yavuz, A. A. Guda, V. Shapovalov, R. Witter, M. Fichtner and H. Hahn, *Phys. Chem. Chem. Phys.*, 2015, **17**, 17288–17295.
2 R. Chen, S. Ren, M. Knapp, D. Wang, R. Witter, M. Fichtner and H. Hahn, *Adv. Energy Mater.*, 2015, **5**, 1401814.
3 C. Baur, I. Källquist, J. Chable, J. H. Chang, R. E. Johnsen, F. Ruiz-Zepeda, J. M. A. Mba, A. J. Naylor, J. M. Garcia-Lastra, T. Vegge, F. Klein, A. R. Schür, P. Norby, K. Edström, M. Hahlin and M. Fichtner, *J. Mater. Chem. A*, 2019, **7**, 21244–21253.
4 I. Källquist, A. J. Naylor, C. Baur, J. Chable, J. Kullgren, M. Fichtner, K. Edström, D. Brandell and M. Hahlin, *Chem. Mater.*, 2019, **31**, 6084–6096.
5 S. Hiroi, K. Ohara and O. Sakata, *Chem. Mater.*, 2021, **33**, 5943–5950.
6 C. Baur, M. E. Lăcătușu, M. Fichtner and R. E. Johnsen, *ACS Appl. Mater. Interfaces*, 2020, **12**, 27010–27016.
7 X. Wang, Y. Huang, D. Ji, F. Omenya, K. Karki, S. Sallis, L. F. J. Piper, K. M. Wiaderek, K. W. Chapman, N. A. Chernova and M. S. Whittingham, *J. Electrochem. Soc.*, 2017, **164**, A1552–A1558.
8 I. Källquist, J. F. Martin, A. J. Naylor, C. Baur, M. Fichtner, J. F. Colin, D. Brandell, K. Edström and M. Hahlin, *J. Phys. Chem. C*, 2020, **124**, 12956–12967.
9 L. Wang, B. Chen, J. Ma, G. Cui and L. Chen, *Chem. Soc. Rev.*, 2018, **47**, 6505–6602.
10 L. Wang, J. Ma, C. Wang, X. Yu, R. Liu, F. Jiang, X. Sun, A. Du, X. Zhou and G. Cui, *Advanced Science*, 2019, **6**, 1900355.
11 X. Li, Y. Qiao, S. Guo, K. Jiang, M. Ishida and H. Zhou, *Adv. Mater.*, 2019, **31**, 1807825.
12 M. A. Cambaz, B. P. Vinayan, H. Geßwein, A. Schiele, A. Sarapulova, T. Diemant, A. Mazilkin, T. Brezesinski, R. J. Behm, H. Ehrenberg and M. Fichtner, *Chem. Mater.*, 2019, **31**, 4330–4340.
13 D. Chen, W. H. Kan and G. Chen, *Adv. Energy Mater.*, 2019, **9**, 1901255.
14 D. Aurbach, B. Markovsky, G. Salitra, E. Markevich, Y. Talyossef, M. Koltypin, L. Nazar, B. Ellis and D. Kovacheva, *J. Power Sources*, 2007, **165**, 491–499.
15 M. Gauthier, T. J. Carney, A. Grimaud, L. Giordano, N. Pour, H. H. Chang, D. P. Fenning, S. F. Lux, O. Paschos, C. Bauer, F. Maglia, S. Lupart, P. Lamp and Y. Shao-Horn, *J. Phys. Chem. Lett.*, 2015, **6**, 4653–4672.
16 K. Xu, *Chem. Rev.*, 2014, **114**, 11503–11618.
17 J. Wu, Y. Yang and W. Yang, *Dalton Trans.*, 2020, **49**, 13519–13527.
18 R. Sharpe, R. A. House, M. J. Clarke, D. Förstermann, J. J. Marie, G. Cibin, K. J. Zhou, H. Y. Playford, P. G. Bruce and M. S. Islam, *J. Am. Chem. Soc.*, 2020, **142**, 21799–21809.
19 H. Ohashi, E. Ishiguro, Y. Tamenori, H. Kishimoto, M. Tanaka, M. Irie, T. Tanaka and T. Ishikawa, *Nucl. Instrum. Methods Phys. Res., Sect. A*, 2001, 529–532.
20 Y. Tamenori, M. Morita and T. Nakamura, *J. Synchrotron Radiat.*, 2011, **18**, 944.
21 V. N. Strocov, T. Schmitt, U. Flechsig, T. Schmidt, A. Imhof, Q. Chen, J. Raabe, R. Betemps, D. Zimoch, J. Krempasky, X. Wang, M. Grioni, A. Piazzalunga and L. Patthey, *J. Synchrotron Radiat.*, 2010, **17**, 631–643.
22 G. Ghiringhelli, A. Piazzalunga, C. Dallera, G. Trezzi, L. Braicovich, T. Schmitt, V. N. Strocov, R. Betemps, L. Patthey, X. Wang and M. Grioni, *Rev. Sci. Instrum.*, 2006, **77**, 113108.
23 M. W. Haverkort, M. Zwierzycki and O. K. Andersen, *Phys. Rev. B: Condens. Matter Mater. Phys.*, 2012, **85**, 165113.
24 M. Retegan, *Crispy: v0.7.4*, 2019, DOI: **10.5281/zenodo.1008184**.
25 F. M. F. de Groot, J. C. Fuggle, B. T. Thole and G. A. Sawatzky, *Phys. Rev. B: Condens. Matter Mater. Phys.*, 1990, **42**, 5459–5468.
26 M. Abbate, H. Pen, M. T. Czyżyk, F. M. F. De Groot, J.-C. Fuggle, Y. J. Ma, C. T. Chen, F. Sette, A. Fujimori, Y. Ueda and K. Kosuge, *J. Electron Spectrosc. Relat. Phenom.*, 1993, **62**, 185–195.
27 S. Nordlinder, A. Augustsson, T. Schmitt, J. Guo, L. C. Duda, J. Nordgren, T. Gustafsson and K. Edström, *Chem. Mater.*, 2003, **15**, 3227–3232.
28 S. M. Bak, R. Qiao, W. Yang, S. Lee, X. Yu, B. Anasori, H. Lee, Y. Gogotsi and X. Q. Yang, *Adv. Energy Mater.*, 2017, **7**, 1700959.
29 R. A. House, L. Jin, U. Maitra, K. Tsuruta, J. W. Somerville, D. P. Förstermann, F. Massel, L. Duda, M. R. Roberts and P. G. Bruce, *Energy Environ. Sci.*, 2018, **11**, 926–932.
30 K. Luo, M. R. Roberts, N. Guerrini, N. Tapia-Ruiz, R. Hao, F. Massel, D. M. Pickup, S. Ramos, Y. S. Liu, J. Guo, A. V. Chadwick, L. C. Duda and P. G. Bruce, *J. Am. Chem. Soc.*, 2016, **138**, 11211–11218.
31 N. Guerrini, L. Jin, J. G. Lozano, K. Luo, A. Sobkowiak, K. Tsuruta, F. Massel, L. C. Duda, M. R. Roberts and P. G. Bruce, *Chem. Mater.*, 2020, **32**, 3733–3740.
32 H. Koga, L. Croguennec, M. Ménétrier, P. Mannessiez, F. Weill, C. Delmas and S. Belin, *J. Phys. Chem. C*, 2014, **118**, 5700–5709.
33 M. Farahmandjou, S. Zhao, W. H. Lai, B. Sun, P. H. Notten and G. Wang, *Nano Mater. Sci.*, 2022, **4**, 322–338.
34 F. D. Groot, *Chem. Rev.*, 2001, **101**, 1779–1808.
35 W. T. Hong, K. A. Stoerzinger, B. Moritz, T. P. Devereaux, W. Yang and Y. Shao-Horn, *J. Phys. Chem. C*, 2015, **119**, 2063–2072.
36 F. Massel, K. Hikima, H. Rensmo, K. Suzuki, M. Hirayama, C. Xu, R. Younesi, Y. S. Liu, J. Guo, R. Kanno, M. Hahlin and L. C. Duda, *J. Phys. Chem. C*, 2019, **123**, 28519–28526.